IEICE TRANS. COMMUN., VOL.E98–B, NO.8 AUGUST 2015

PAPER

An Approach to Evaluate Electromagnetic Interference with a Wearable ECG at Frequencies below 1 MHz

Wei LIAO[†a)], ***Nonmember***, **Jingjing SHI**[†b)], ***Member***, ***and*** **Jianqing WANG**[†c)], ***Fellow***

SUMMARY In this study, we propose a two-step approach to evaluate electromagnetic interference (EMI) with a wearable vital signal sensor. The two-step approach combines a quasi-static electromagnetic (EM) field analysis and an electric circuit analysis, and is applied to the EMI evaluation at frequencies below 1 MHz for our developed wearable electrocardiogram (ECG) to demonstrate its usefulness. The quasi-static EM field analysis gives the common mode voltage coupled from the incident EM field at the ECG sensing electrodes, and the electric circuit analysis quantifies a differential mode voltage at the differential amplifier output of the ECG detection circuit. The differential mode voltage has been shown to come from a conversion from the common mode voltage due to an imbalance between the contact impedances of the two sensing electrodes. When the contact impedance is resistive, the induced differential mode voltage increases with frequency up to 100 kHz, and keeps constant after 100 kHz, i.e., exhibits a high pass filter characteristic. While when the contact impedance is capacitive, the differential mode voltage exhibits a band pass filter characteristic with the maximum at frequency of around 150 kHz. The differential voltage may achieve nearly 1 V at the differential amplifier output for an imbalance of 30% under 10 V/m plane-wave incident electric field, and completely mask the ECG signal. It is essential to reduce the imbalance as much as possible so as to prevent a significant interference voltage in the amplified ECG signal.

key words: *electromagnetic interference (EMI), wearable electrocardiogram (ECG), sensing electrode, common mode voltage, differential mode voltage, quasi-static approximation*

1. Introduction

Today's aging population is leading to a wide-scale demand for health-state monitoring in hospital and at home. Wireless wearable health-state monitoring can effectively reduce the inconvenience of wire links, and save time and resources. As a typical usage, the wireless wearable device is a vital signal sensor with communication function for collecting blood pressure, electrocardiogram (ECG), electroencephalogram (EEG) data, and so on. By attaching such devices to patients or elderly people, the vital signal data can be automatically collected, and then forwarded to medical staff in a hospital or medical center for medical and health care administration and applications [1]–[4]. In a wearable ECG, a sensor is placed on the human body to collect the ECG data and the collected data are sent to a data server by wireless communication. The data server may be a cellular phone or a personal computer (PC) for further processing and display. It also has the ability to store the data for further examination by a health care professional.

However, the increasing electromagnetic (EM) wave applications imply a potential of electromagnetic interference (EMI) with a wearable ECG. So far, the EMI problems for medical devices are often investigated in hospital in mobile communication frequency bands [5]. For wearable health care devices such as a wearable ECG, the EMI problem is mainly focused on the interference in commercial power frequency bands [6], [7]. In fact, near the ECG signal frequencies, there are many frequency bands below 1 MHz being used for not only the commercial power supply, but also broadcast, electronic security check, as well as wireless power transfer [8], [9]. The EM fields in these frequencies can couple into the wearable ECG through the sensing electrodes to cause an an interference voltage in the ECG signals. But to our knowledge, there is no study about how to quantify such interferences. In this study, therefore, we propose a two-step approach for evaluating the EMI level at the wearable ECG. In the first step, we calculate the EMI voltages induced between the ECG sensing electrodes and the ground as a common mode voltage by EM field simulations, while in the second step, we evaluate the interference voltage with ECG signals by an electric circuit analysis or simulation. Such an approach provides an effective means to quantitatively evaluate the EMI for a wearable health care device in the design stage.

This paper demonstrates this approach in quantifying the EMI performance for our developed wearable ECG to show its usefulness. Based on the analysis results, some design guidelines are also derived for EMI suppression. It should be noted that the ECG detection circuit in our wearable ECG has a typical structure as introduced in [4]. So the derived findings are general to some extent, and applying this two-step approach to other wearable ECGs or health care devices is straightforward.

2. Block Diagram of Wearable ECG

Figure 1 shows the block diagram of the wearable ECG developed in our laboratory [10]. The ECG sensor is composed of two 3 cm × 3 cm square electrodes. The two electrodes are attached to the chest directly or through a capacitive coupling, respectively, for ECG signal acquisition. It should be noted that, except for the two signal electrodes, a ground electrode is often attached to the human body as a reference. However, in our developed wearable ECG, the

Manuscript received December 26, 2014.
Manuscript revised March 19, 2015.

[†]The authors are with the Graduate School of Engineering, Nagoya Institute of Technology, Nagoya-shi, 466-8555 Japan.
a) E-mail: liao.wei@nitech.ac.jp
b) E-mail: shi.jingjing@nitech.ac.jp
c) E-mail: wang@nitech.ac.jp

DOI: 10.1587/transcom.E98.B.1606

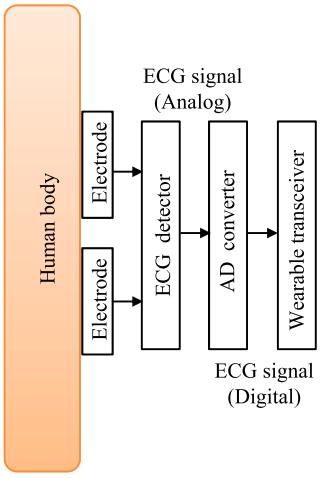

Fig. 1 Block diagram of the wearable ECG.

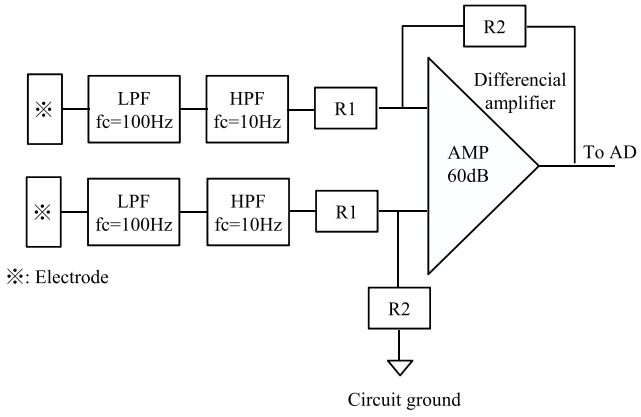

Fig. 2 Structure of the ECG detection circuit.

ground electrode is removed to reduce system complexity. Such a simplified structure has also been reported in the literature [11]. The ECG signals acquired from the two sensing electrodes are then filtered and differentially amplified with an operational amplifier (opamp) as shown in Fig. 2. The low pass filter (LPF) and high pass filter (HPF) are used respectively to remove the direct-current (DC) component, the drift noises, and high frequency interference noises. Both of the LPF and HPF are composed of the second-order RC filters. They have a cutoff frequency of 100 Hz for the LPF and 10 Hz for the HPF, respectively, and an attenuation of 30 dB outside the pass bands. A notch filter is also useful to cut the commercial power frequency of 50 or 60 Hz. The circuit amplifies differentially the signals coming from the two sensing electrodes and adjust their levels to fall into the analog input range of an analog-to-digital converter (ADC) with a sampling frequency of 500 Hz and quantization of 10 bits. The AD-converted ECG signals are transmitted by a wireless technology such as Bluetooth or human body communication (HBC) in our case.

Figure 3 shows a typical example of the ECG signal acquired by our wearable ECG. As can be seen, although the weaker P-wave and T-wave are not observed, the wearable ECG clearly acquires the Q-wave, R-wave and S-wave with reasonable accuracy, and so can be used to monitor the health conditions of human. The R-wave exhibits a voltage level in the order of several mV. When the R-wave peak voltage is in the order of 1 mV, the Q-wave and S-wave are in the order of 0.3 mV and 0.6 mV, respectively. The main frequency components of the ECG signal falls in the range of several Hz to several hundred Hz. With improved sensitivity of the sensing electrodes and detection circuit, we have confirmed that our wearable ECG is available to detect the P-wave and T-wave.

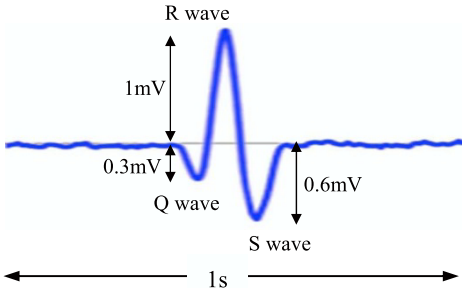

Fig. 3 Example of ECG signal acquired by our developed wearable ECG.

3. EMI Evaluation

The wearable ECG may be interfered by environmental EM fields through the two sensing electrodes on the chest. Except for the commercial power frequency, the low frequency (LF) and middle frequency (MF) band signals are also easily coupled into the ECG detection circuit because they are near the ECG's working frequencies. Let us consider a human standing on a ground plane, the incident EM field will induce a common mode voltage between the human body and the ground since the human body is approximately a conductor at these frequencies. The common mode voltage is actually an EM-field-induced voltage offset which is "common" to both the two input electrodes, and cannot be rejected by the differential stage. The common mode voltage is therefore an interference with the ECG detection circuit. If it appears at the output of the ECG detection circuit, it will cause an EMI problem. Therefore, to make an EMI evaluation for the wearable ECG, we need a two-step approach. The first step is an EM field approach to determine the common mode voltage under the considered frequencies, and the second step is an electronic circuit approach to determine the interference voltage appearing in the amplified ECG signals.

3.1 EM Field Approach

Figure 4 shows a numerical model with a human body standing on a ground plane, irradiated by a uniform EM field. The EM field is a plane-wave incidence from the front of the human body with the electric field along the height direction. The numerical human body model was developed based on

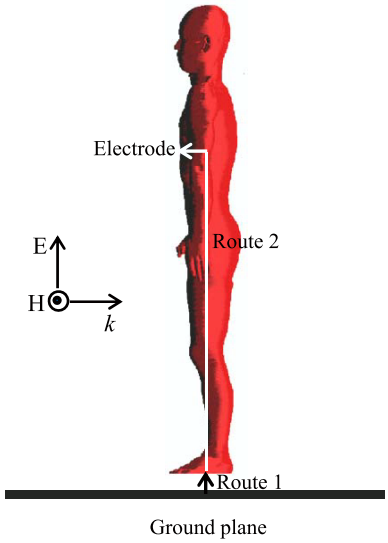

Fig. 4 Numerical model with a human body standing on a ground plane, and the integration route 1 and 2 to obtain the common mode interference voltage.

anatomical magnetic resonance imaging data [12], and the finite difference time domain (FDTD) method was adopted as the numerical EM field analysis tool in view of its flexibility in modeling complex human body shapes. When the frequencies are below 1 MHz, the size of the human body is smaller than the wavelength, and $|\sigma + j\omega\varepsilon| >> \omega\varepsilon_0$ where σ and ε are the conductivity and the permittivity of the human tissues, respectively, ω is the angular frequency, and ε_0 is the permittivity of free space. Under these conditions, the quasi-static approximation is valid so that the electric field outside the human body depends not on the internal tissue properties but only on the shape of the body. This makes that the total electric field outside the human body $E_{Air}(f)$ is normal to the body surface, and is related to the electric field inside the human body $E_{Body}(f)$ by the boundary conditions as [13]

$$j\omega\varepsilon_0\hat{n} \cdot E_{Air}(f) = (\sigma + j\omega\varepsilon)\hat{n} \cdot E_{Body}(f) \quad (1)$$

where f is the frequency, and $\hat{n}$ denotes the normal direction to the human body surface. If we employ a higher quasi-static frequency f' to irradiate the human body, the calculated electric field $E_{Body}(f')$ can be then scaled back to frequency f of interest. From Eq. (1) we can write

$$E_{Body}(f) \cong \frac{f\sigma'}{f'\sigma} E_{Body}(f') \quad (2)$$

under the assumption that $\sigma + j\omega\varepsilon \cong \sigma$ at both f and f'. This method gives the electric fields inside the human body at frequency f of interest from the result at a higher frequency f', for example, 10 MHz, to reduce the FDTD computation time. This is because that the FDTD method needs to calculate iteratively in the time domain until a convergence is reached, while the scaling to a higher frequency can effectively reduces the needed number of iterations.

However, our purpose is to obtain the induced common mode voltage between the electrodes and the ground plane. This can be calculated by integrating the electric field along a route from the ground plane to the feet (route 1) and from the feet to the electrodes (route 2), as shown in Fig. 4. The route 2 passes through the inside of the human body since the above-described FDTD method gives the electric fields inside the body at f. For the electric field outside the body $E_{Air}(f)$ along the route 1, i.e., between the feet and the ground plane, it can be obtained from Eq. (1) because $E_{Body}(f)$ is known. The employment of such an approach is because that the frequency scaling technique is valid and well examined just for the electric field inside the human body $E_{Body}(f)$. It's accuracy is unclear for the electric field outside the human body. We thus first used the frequency scaling to obtain $E_{Body}(f)$ and then used Eq. (1) to obtain $E_{Air}(f)$. In such a way, we can obtain the voltages between the two electrodes and the ground plane, respectively, which are resulted from the incident EM field and are EM interferences with the ECG detection circuit. Since the human body is approximately a conductor at frequencies below 1 MHz, the induced interference voltages at the two electrode locations are almost identical so that they can be directly added to the input of the ECG detection circuit as a common mode voltage.

In the FDTD simulation to determine the common mode EMI voltage, we approximated the human body model as a homogeneous one with the dielectric properties of muscle [14]. The human body model was assumed to stand on the ground plane with a spacing of 1 cm. The two sensing electrodes were attached to the left chest with a spatial interval of 3 cm between them. Due to the approximate conductor property of the human body at the investigated frequencies, the circuitry or other electrodes attached to the human body in a small area did not result in a significant influence on the calculated common mode voltage. The full FDTD simulation was run at $f' = 10$ MHz, with a voxel size from 0.25 cm to 4 cm, and the iterations up to 10 time periods. Perfect matched layers (PML) boundary conditions were employed. Fig. 5 shows the FDTD-simulated electric field distribution at 10 MHz. As can be seen, the electric fields surround the body surface in the outside of the human body, and are quite weak inside the human body. Using the frequency scaling from the FDTD simulation results at $f' = 10$ MHz, we then obtained the common mode voltages V_{c1} and V_{c2} at various frequencies below 1 MHz between each electrode attachment location on the human body and the ground plane. There is almost no difference between V_{c1} and V_{c2}, which can be attributed to the approximate conductor performance of the human body at frequencies below 1 MHz. So we assume that $V_{c1} = V_{c2} = V_c$ and consider it as the voltage between the human body and the ground plane. This fact suggests that the quasi-static approximation is reasonable at these investigated frequencies. In order to further verify the common mode voltage scaled from that at 10 MHz, we also run a full FDTD calculation at 1 MHz and calculated the common mode voltage directly. The result

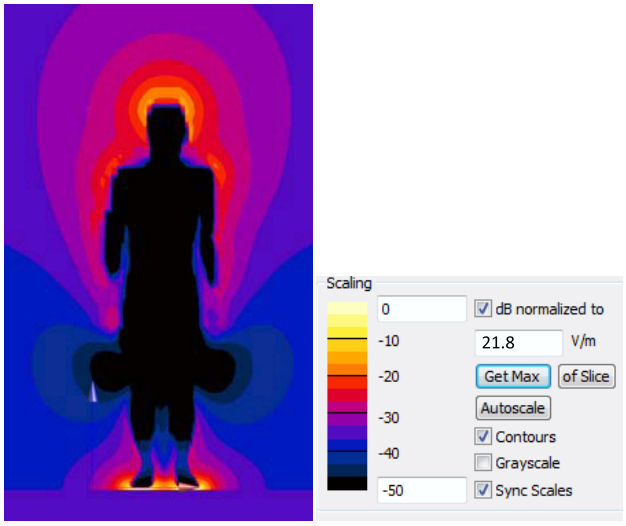

Fig. 5 FDTD-simulated electric field distribution at 10 MHz. The incident plane-wave electric field strength is 1 V/m.

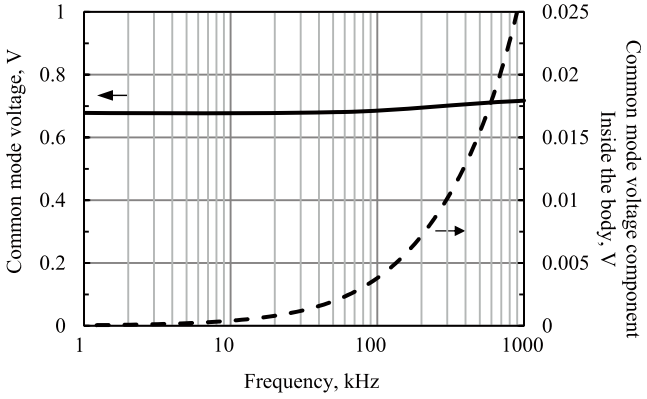

Fig. 6 Common mode interference voltages at the electrodes as a function of frequency under 1 V/m plane-wave incident electric field strength.

exhibited good agreement with the frequency scaling one in an accuracy of 10%. So the common mode interference voltage calculated in this approach is reliable.

Figure 6 shows the common mode voltage V_c as a function of frequency. It can be found that the common mode voltage component from the route 2 inside the human body is very small and increases with frequency, while the total common mode voltage is almost flat with respect to frequency. For a 1 V/m plane-wave incident electric field (root mean square value), the induced common mode voltage between the human body and the ground plane is nearly 0.7 V. It should be noted that this voltage is caused by not only the electric filed but also the magnetic field. If we only consider the effect of electric field or magnetic filed, the induced voltage will be smaller than this level.

3.2 Electronic Circuit Approach

To investigate the influence of the induced common mode interference voltage on ECG signals, the ECG detection circuit in Fig. 2 can be re-written equivalently as Fig. 7. The interference voltage V_c is between the electrodes and the ground plane, here we denotes which as the earth ground. When the two sensing electrodes touch the human body directly, there will be a contact resistance R_{ea} or R_{eb} between each electrode and the body. While when the two sensing electrodes do not touch the human body directly, there will be a coupling capacitance C_{ea} or C_{eb} between each electrode and the body. In any case, we denote them as contact impedance Z_{ea} and Z_{eb} respectively. The two contact impedances are usually imbalanced due to the different attachment conditions, which results in a differential output at the differential amplifier. On the other hand, the input impedance Z_{in} at the plus input and minus input are almost the same for a well designed opamp. This makes the imbalance in the contact impedances become the main reason to change the common mode input voltage into a differential mode interference voltage at the output of the differential amplifier.

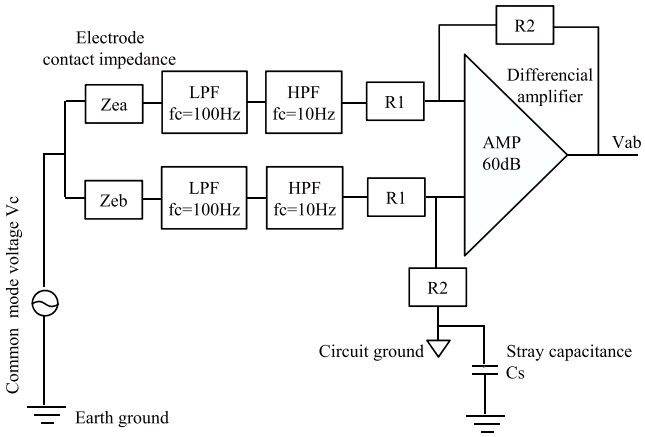

Fig. 7 Equivalent circuit for investigating the EMI influence of the common mode interference voltage.

From Fig. 7, based on the differential amplifier circuit theory, the differential output voltage V_{ab} for an ideal opamp can be written as

$$V_{ab} = \frac{R_2(Z_{ea} - Z_{eb})}{(Z_{ea} + Z_{eb} + 2R_1)Z_{cs} + (Z_{ea} + R_1)(Z_{eb} + R_1 + R_2)} V_c \tag{3}$$

where $Z_{cs} = 1/j\omega C_s$, and C_s is a stray capacitance between the isolated ECG circuit ground and the earth ground. Using the calculated common mode voltage in Fig. 6 as the input to the equivalent circuit in Fig. 7, we can calculate the differential mode interference voltage V_{ab} using Eq. (3). In addition, using a circuit simulation tool such as SPICE to obtain the interference voltage at the output of differential amplifier is also an effective approach. It is obvious that the differential mode interference V_{ab} will be zero if the two contact impedances Z_{ea} and Z_{eb} are balanced.

4. Results and Discussion

To clarify the influence of the imbalance of the contact

Table 1 Circuit parameters.

R_e, average of R_{ea} and R_{eb}	10 kΩ–100 kΩ
C_e, average of C_{ea} and C_{eb}	30 pF–300 pF
Z_{in}, input impedance	100 MΩ
R_1	5 kΩ
R_2	5 MΩ
Differential amplifier gain	60 dB
C_s	20 pF–200 pF
LPF cutoff freq.	100 Hz
HPF cutoff freq.	10 Hz
Attenuation outside pass band	60 dB

impedances, we first make some assumptions for simplifying the discussion without losing generality. As shown in Fig. 3, the ECG signal is in the order of around 1 mV. It usually passes a LPF and a HPF, and is then amplified about 60 dB to achieve around 1 V for AD converter. On the other hand, the noises are usually removed by the LPF and HPF which have an attenuation also in the order of 60 dB. So in the following discussion, we assume that both the gain of the differential amplifier and the attenuation of the LPF and HPF take a typical value of 60 dB. This makes that

- the ECG signal is amplified 60 dB to be in the order of 1 V;
- the common mode noises are first attenuated 60 dB by the LPF and HPF and are then amplified 60 dB by the differential amplifier, so that they change actually 0 dB. This means that $R_1 = R_2$ in Fig. 7 and Eq. (3), i.e., the amplification factor is one.

Table 1 summarizes the parameters used in discussion for the circuit shown in Fig. 7. When the sensing electrodes are touched directly to the human body, the contact resistances R_{ea} and R_{eb} were assumed between 10 kΩ and 100 kΩ based on the literature [6]. When the sensing electrodes are not touched directly to the human body, the coupling capacitances C_{ea} and C_{eb} were calculated between 30 pF and 300 pF based on their sizes and the spatial interval from the body surface (from 0.1 mm to 1 mm). As for C_s, the capacitance between the circuit ground and the earth ground, in view of that the circuit is attached to the human body, we assumed it between 20 pF and 200 pF [7].

In order to quantify the common mode voltage caused by the imbalance of the contact impedances between Z_{ea} and Z_{eb}, we changed R_{ea} and R_{eb}, or C_{ea} and C_{eb}, to have an imbalance up to 30% at their average value. An imbalance of 10%, for example, means that $Z_{ea} = 9$ kΩ and $Z_{eb} = 11$ kΩ for an average value of 10 kΩ. Figure 8 shows the common mode interference voltage V_{ab} calculated from Eq. (3), under a 10 V/m plane-wave incident electric field strength. In radiated immunity tests, a 10 V/m incident electric field is usually used as a special (higher) test level for the EM field irradiation from 80 MHz to 1 GHz [15]. Here we referred this test level but at the frequencies below 1 MHz. In addition, we also conducted a circuit simulation with SPICE for the same circuit in Fig. 7, and plotted the simulated result in Fig. 8. As can be seen, the calculated common mode voltages agree well with the SPICE simulated ones. This ensures the validity and usefulness of both Eq. (3) and SPICE simulation in quantifying the EMI interference voltages.

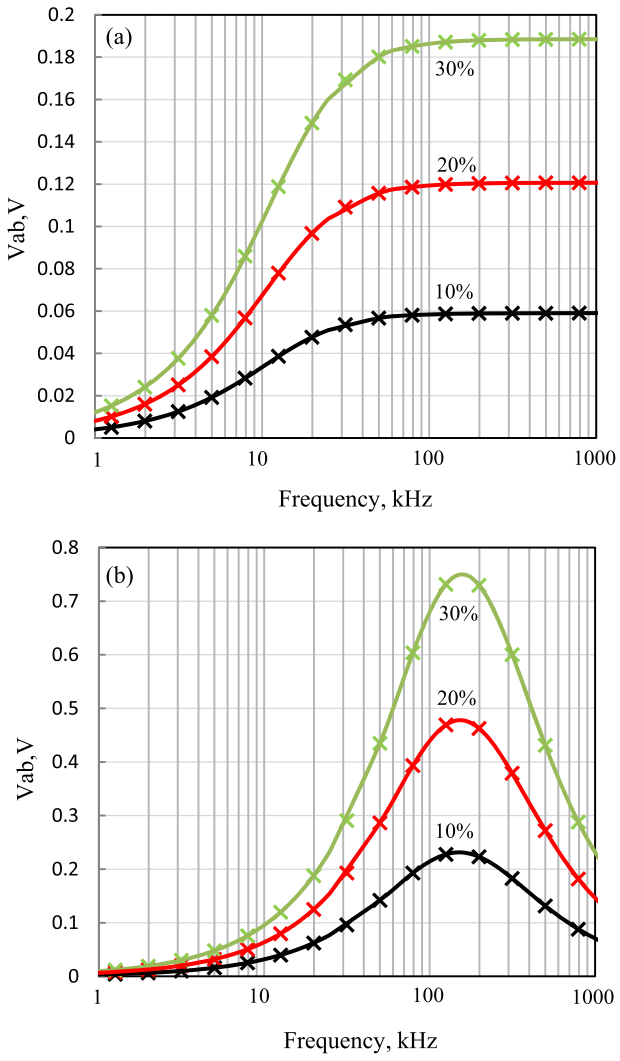

Fig. 8 Calculated and SPICE-simulated interference voltages at the output of the differential amplifier as a function of frequency under 10 V/m plane-wave incident electric field strength. The imbalances of the contact impedance are 10%, 20% and 30%, respectively. (a) imbalance of contact resistances at an average value of 100 kΩ, (b) imbalance of coupling capacitances at an average value of 300 pF. Solid line: calculated from Eq. (3); symbol: SPICE.

From Fig. 8(a), it can be found that the differential interference voltage V_{ab}, which is induced by the common mode voltage V_c due to the imbalance of the contact resistances between R_{ea} and R_{eb}, increases with frequency between 1 kHz and 100 kHz, and keeps constant after 100 kHz, i.e., exhibits a high pass filter characteristic. It may achieve nearly 0.2 V above 100 kHz when the imbalance is 30% for an average contact resistance $R_e = 100$ kΩ. On the other hand, from Fig. 8(b), the differential interference voltage V_{ab} induced by the imbalance of the coupling capacitances between C_{ea} and C_{eb} exhibits a band pass filter characteristic with the maximum at frequency of around 150 kHz. The maximum value should be determined by the stray capaci-

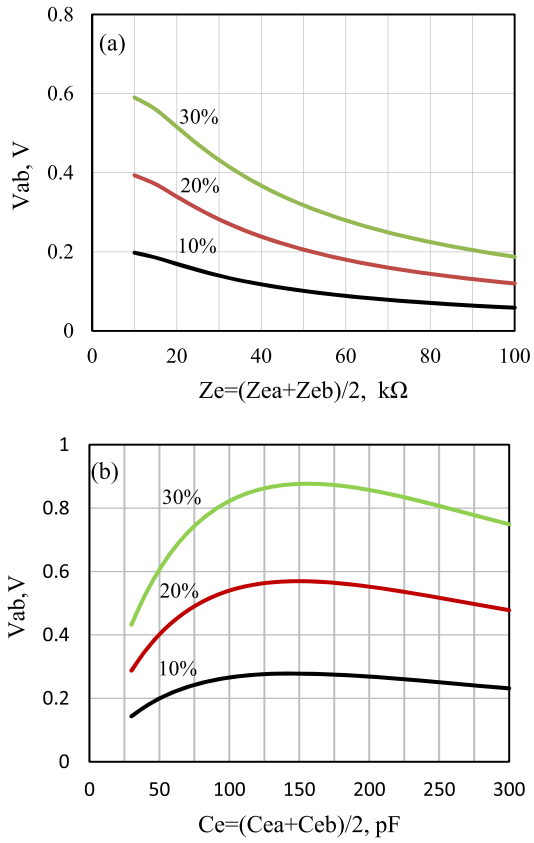

Fig. 9 Influence of the average contact impedance Z_e on the interference voltage V_{ab} under 10 V/m plane-wave incident electric field strength. (a) for contact resistance, (b) for coupling capacitance.

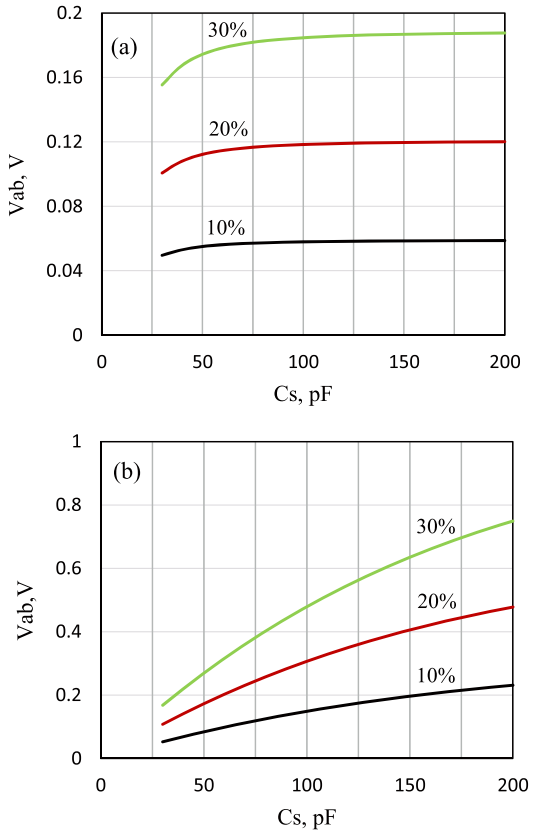

Fig. 10 Influence of the stray capacitance C_s on the interference voltage V_{ab} under 10 V/m plane-wave incident electric field. (a) Contact resistance Z_e = 100 kΩ., (b) coupling capacitance C_e = 300 pF.

tance C_s, and the corresponding frequency may shift with the value of C_s. Again, V_{ab} achieves 0.8 V at maximum when the imbalance is 30% for an average coupling capacitance C_e = 300 pF. These interference voltage levels are at the same order as the amplified Q-wave, S-wave and R-wave in the ECG signal (referring to Fig. 3), and can be a significant interference to mask the ECG signals.

Figure 9 shows the influence of the average contact impedance Z_e on the interference voltage V_{ab} at 145 kHz, which is a candidate frequency for wireless power transfer, and at which a peak interference voltage is observed for capacitively coupling electrodes as shown in Fig. 8(b). Figure 9(a) exhibits that V_{ab} increases with the decrease of contact resistance. That is to say, the imbalance effect is more sensitive for smaller contact resistance. When the average contact resistance is 10 kΩ with an imbalance of 30%, the interference voltage V_{ab} may achieve 0.6 V under the 10 V/m plane-wave incident electric field strength. On the other hand, Fig. 9(b) exhibits that V_{ab} has a maximum when changing the coupling capacitance. When the average coupling capacitance is 300 pF with an imbalance of 30%, the interference voltage V_{ab} may achieve nearly 1 V under the 10 V/m plane-wave incident electric field strength. These results again suggest that the induced interference voltage may mask the Q-wave and S-wave completely and is even possible to mask the R-wave so that the heart rate cannot be detected.

Moreover, we also investigated the influence of the stray capacitance C_s on the interference voltage V_{ab} at 145 kHz. It is found that V_{ab} is insensitive to the change of C_s for contact resistance as shown in Fig. 10(a), but it becomes larger with the increase of C_s as shown in Fig. 10(b). The smaller stray capacitance will contribute to a smaller interference voltage output.

From the above results, it is clarified that when the imbalance between the contact impedance of the two electrodes is larger than 30%, the interference voltage V_{ab} due to the common mode voltage caused by the plane-wave incident electric field at 10 V/m may achieve a significant level to affect the ECG signal, for example, mask the Q-wave, S-wave and even R-wave. To suppress such interferences, one should

- reduce the imbalance of contact impedance as much as possible, because it is the main reason to cause an interference voltage at the differential amplifier output;
- increase the attenuation outside the pass band (larger than 60 dB) for the LPF and HPF. Moreover, employ a band elimination filter (BEF) to remove the common mode voltage at a specific frequency.

Moreover, it should also be a useful means to introduce

a variable impedance after the electrodes. One may adjust the variable impedance, based on the detected amount of imbalance between the two electrodes, to make the two electrodes at a balance state.

5. Conclusion

Electromagnetic compatibility (EMC) consideration is essential in designing a wireless wearable vital signal monitoring system. At frequencies below 1 MHz, the EM field couples especially easily with vital signal detection circuits and causes an interference to the detected signal. To evaluate the interference voltage level against the incident EM field intensity, we have proposed a two-step approach, which combines a quasi-static EM field analysis and an electric circuit analysis. In the quasi-static EM field analysis, we employ the FDTD method with a frequency scaling technique to calculate the common mode interference voltage which couples into the input of the ECG detection circuit. While in the electric circuit analysis, we employ SPICE to calculate the differential mode voltage at the differential amplifier output. This two-step approach first time provides an effective means to quantitatively evaluate the EMI for a wearable health care device in the design stage. It has been applied to our developed wearable ECG to demonstrate its validity and find some basic design guidelines. As a result, we have found that the main reason for changing the common mode interference voltage into a differential mode interference voltage is due to an imbalance between the contact impedances of the two sensing electrodes. When the contact impedance is resistive, the induced differential mode voltage exhibits a high pass filter characteristic. It increases with frequency up to 100 kHz, and keeps constant after 100 kHz. While when the contact impedance is capacitive, the differential mode voltage exhibits a band pass filter characteristic with the maximum at frequency of around 150 kHz. The differential voltage may achieve nearly 1 V at the differential amplifier output for an imbalance of 30% under 10 V/m plane-wave incident electric field, and completely mask the ECG signal. To suppress such interferences, the imbalance between the two contact impedances should be reduced as much as possible, and the attenuation outside the pass bands of the LPF and HPF should be larger than 60 dB.

A future subject is the optimum design of our wearable ECG from the EMC point of views based on the above findings.

Acknowledgement

This study is supported in part by the Grant-in-Aid for Scientific Research (Grant No. 24560452).

References

[1] J. Wang and Q. Wang, Body Area Communications, Wiley-IEEE, 2013.
[2] A.W. Astrin, H.-B. Li, and R. Kohno, "Standardization for body area networks," IEICE Trans. Commun., vol.E92-B, no.2, pp.366–372, Feb. 2009.
[3] E. Montón, J.F. Hernandez, J.M. Blasco, T. Hervé, J. Micallef, I. Grech, A. Brincat, and V. Traver, "Body area network for wireless patient monitoring," IET Commun., vol.2, no.2, pp.215–222, Feb. 2008.
[4] E. Nemati, M. Deen, and T. Mondal, "A wireless wearable ECG sensor for long-term applications," IEEE Commun. Mag., vol.50, no.1, pp.36–43, Jan. 2012.
[5] A. Baranchuk, J. Kang, C. Shaw, D. Campbell, S. Ribas, W.M. Hopman, H. Alanazi, D.P. Redfearn, and C.S. Simpson, "Electromagnetic interference of communication devices on ECG machines," Clin. Cardiol., vol.32, no.10, pp.588–592, Oct. 2009.
[6] E.M. Spinelli, N.H. Martinez, and M.A. Mayosky, "A transconductance driven-right-leg circuit," IEEE Trans. Biomed. Eng., vol.46, no.12, pp.1466–1470, Dec. 1999.
[7] A.C.M. van Rijn, A. Peper, and C.A. Grimbergen, "High-quality recording of bioelectric events," Med. Biol. Eng. Comput., vol.28, no.5, pp.389–397, Sept. 1990.
[8] F. Musavi and W. Eberle, "Overview of wireless power transfer technologies for electric vehicle battery charging," IET Power Electronics, vol.7, no.1, pp.60–66, Jan. 2014.
[9] L. Xie, Y. Shi, Y.T. Hou, and A. Lou, "Wireless power transfer and applications to sensor networks," IEEE Wireless Commun., vol.20, no.4, pp.140–145, Aug. 2013.
[10] T. Kato, J. Sakuma, D. Anzai and J. Wang, "Reliability evaluation of ECG signal transmitted by IR-based human body communication," IEICE Technal Report, EMCJ2014-20, July 2014.
[11] S. Ha, C. Kim, Y.M. Chi, A. Akinin, C. Maier, A. Ueno, and G. Cauwenberghs, "Integrated circuits and electrode interfaces for noninvasive physiological monitoring," IEEE Trans. Biomed. Eng., vol.61, no.5, pp.1522–1537, May 2014.
[12] T. Nagaoka, S. Watanabe, K. Sakurai, E. Kunieda, S. Watanabe, M. Taki, and Y. Yamanaka, "Development of realistic high-resolution whole-body voxel models of Japanese adult males and females of average height and weight, and application of models to radio-frequency electromagnetic-field dosimetry," Phys. Med. Biol., vol.49, no.1, pp.1–15, Jan. 2004.
[13] O.P. Gandhi and J.-Y. Chen, "Numerical dosimetry at power-line frequencies using anatomically based models," Bioelectromagnetics, vol.13, no.S1, pp.43–60, 1992.
[14] http://niremf.ifac.cnr.it/tissprop/
[15] International Standard IEC61000-4-3, Electromagnetic compatibility — Part 4-3: Testing and measurement techniques — Radiated, radio-frequency, electromagnetic field immunity test, Feb. 2006.

Wei Liao received the B.E. degree in electronic information engineering from Nanchang University, Nanchang, China, in 2003, and the M.E. and D.E. degrees from East China Normal University, Shanghai, China, in 2007 and 2010, both in communication and information system. From 2003 to 2004, she was a Lecturer with the Department of information Engineering, Jiangxi University of Technology, Ganzhou, China. Since 2010, she has been a Postdoctoral Fellow with the Nagoya Institute of Technology, Nagoya, Japan, where she is involved in research on electromagnetic compatibility and biomedical communications.

Jingjing Shi received the B.E. degree from Shenyang University of Chemical Technology, Shenyang, China, in 2007, and the M.E. and D.E. degrees from Nagoya Institute of Technology, Nagoya, Japan, in 2010 and 2013, respectively. She is currently at Nagoya Institute of Technology as a Postdoctoral Research Associate. Her research interests involve biomedical communications in wireless communication networks and biomedical EMC.

Jianqing Wang received the B.E. degree in electronic engineering from Beijing Institute of Technology, Beijing, China, in 1984, and the M.E. and D.E. degrees in electrical and communication engineering from Tohoku University, Sendai, Japan, in 1988 and 1991, respectively. He was a Research Associate at Tohoku University and a Senior Engineer at Sophia Systems Co., Ltd., prior to joining Nagoya Institute of Technology, Nagoya, Japan, in 1997, where he is currently a Professor. His research interests include biomedical communications and electromagnetic compatibility.